Mechanistic Study of the Electrochemical Reduction of CO_2 in Aprotic Ionic Liquid in Air*

Go IIJIMA Kyosuke SUGIURA Kenichi MORISHITA
Hajime SHINGAI Junichi NARUSE Hiroaki YOTO

The capture and electrochemical conversion of dilute CO_2 in air is a promising approach to mitigate global warming. Aiming to increase the efficiency of the electrochemical reduction of CO_2, we fabricated electrodes and developed a custom-designed sealed electrochemical reaction system to study the mechanism of this conversion. The performance of three metal electrodes, Ag, Cu, and SUS 316 L, was compared in an aprotic ionic liquid as the electrolyte to monitor the CO_2 concentration and chemical reactions using a CO_2 sensor and diffuse reflectance infrared Fourier transform spectroscopy and Raman spectroscopy in CO_2/N_2 (400 ppm CO_2 and 99.96% N_2) or synthetic air (400 ppm CO_2, 21% O_2, and 79% N_2). The CO_2 concentration decreased at negative potentials and was more drastic in synthetic air than in CO_2/N_2. At negative potential in synthetic air, IR revealed carbon monoxide, carbonate, or peroxydicarbonate on the Ag, Cu, or SUS 316L electrodes, respectively. Reaction intermediates were identified using Raman spectroscopy. Superoxide ($O_2^{\bullet -}$), produced by the reduction of O_2 on each electrode, promotes the electrochemical reduction of CO_2 whose reduction potential is higher on the negative side than that of O_2. This research deepens our understanding of the electrochemical capture/release and conversion of dilute CO_2.

Keywords :
Electrochemical CO_2 reduction, Dilute CO_2, Superoxide, Aprotic ionic liquid, DRIFTS, Raman

Introduction

Global warming has become an international issue in recent years, and it is necessary to mitigate the accumulation of CO_2 in the air as one of the causes of the problem[1]. Although many methods are being considered to address this problem, electrochemical CO_2 capture and/or reduction are promising methods because they are able to utilize electricity that is sustainably generated from wind power or solar power[2]. In recent years, technology to capture dilute CO_2 in air, known as direct air capture (DAC), has been attracting considerable attention because conventional CO_2 capture techniques, which target high-concentration CO_2, have reached their limits in terms of the reduction of CO_2[3]. Among the DAC techniques, electric-swing adsorption (ESA), can limit the energy losses because the adsorbent materials can be operated at relatively high efficiency[4]. Studies investigating the direct conversion of CO_2 in air are also underway to improve the efficiency by combining CO_2 capture and conversion[5]. However, these methods are problematic in many ways, especially because of the low Faradaic efficiencies resulting from the sluggish CO_2 conversion due to the side reaction of the aqueous electrolyte to produce hydrogen[5]. Given the circumstances, investigations concerned with the electrochemical CO_2 capture and/or reduction in aprotic solution are gradually producing exciting results. For example, Voskian et al. reported an ESA system using an electrode comprising redox-active organic compounds in an ionic liquid (IL) as the aprotic electrolyte. They captured dilute CO_2 efficiently with a high electron utilization rate (i.e., mole of CO_2 per mole of electrons) that exceeded 90%[4]. With respect to CO_2 conversion, studies with Li-CO_2 batteries are the most common. Qiao et al. presented highly efficient electrochemical reactions to achieve energy-efficient CO_2 fixation of 73.3%[6]. Other researchers studied electrochemical CO_2 reduction for reusable fuel production; for example, an aprotic solution was used for the production of oxalate using a Pb electrode with high Faradaic efficiencies of approximately 70%[7]. The production of carbon monoxide (CO) on a Zn electrode in combination with the Li cation generated from the counter electrode (C.E.) was also reported by Xie et al[8]. Based on these studies, the products from the reduction of CO_2 in aprotic solution evidently depend on the electrode species, which were summarized previously[9]. They reported that oxalate is likely to be produced on Pb, Tl, or Fe as representative, whereas CO evolution occurs on other electrodes such as Ag, Zn, or Sn. The other product is hydrogen, which presumably stems from a side reaction of electrochemical CO_2 reduction, and is deduced to be generated by the splitting of H_2O as a contaminant in solution or the decomposition of aprotic solutions. Bagger et al., who sought to determine whether the products were related to the metal electrodes, found that the products depended on the reaction kinetics of the electrochemical CO_2 reduction intermediates[9].Despite the progress made by studying CO_2 reduction in aprotic solution, these studies mainly used 100% CO_2. However, to ensure the electrochemical cell mimics the natural environment, the evaluation should be conducted in a mixture of CO_2 and O_2. However, the electrochemical reduction of CO_2 in a mixed atmosphere is immature and studies are currently underway[10-21]. The first electrochemical reduction of CO_2 in combination with O_2 to form carbonate by Takechi et al., indicated that reduced O_2 (superoxide, $O_2^{\bullet -}$) promotes CO_2 reduction and enhances the discharge capacity of a Li-CO_2 battery[18]. Other studies involving Li-CO_2 batteries in combination with O_2 were reported[16,17,21]. Other than these studies, Halilu et al. investigated the electrochemical conversion of CO_2 and O_2 in an aprotic ionic liquid with peroxydicarbonate as the product[12]. Although remarkable progress has been made, the mechanism of CO_2 reduction in combination with O_2, particularly the reaction routes or intermediates, are not well understood. In our previous attempts to clarify the mechanism of electrochemical CO_2 capture or reduction using in situ FT-IR analyses, we succeeded in monitoring CO_2 conversion under several conditions[22]. This motivated us to additionally observe the CO_2 behavior on the electrode using in situ spectrometry under aprotic conditions in atmospheric air in much greater detail than before.

In this study, we evaluated Ag, Cu, and SUS 316L metal electrodes to attempt to unravel the mechanism of the electrochemical reduction of CO_2 and O_2 in an aprotic ionic liquid. Cyclic voltammetry (CV)

* This article was published in ChemSusChem, 2025, 18, e202401832, Copyright Wiley

measurements with these electrodes determined the difference in their reduction potentials. In addition, we developed an atmosphere control electrochemical measuring system (***ACEMS***) to enable us to measure the CO_2 concentration in the electrochemical device and simultaneously conduct in situ spectroscopic measurements (FT-IR or Raman) during potential step chronoamperometry (PSC). These spectroscopic measurements revealed the different reaction routes, reaction intermediates, and products on each electrode.

Experimental Procedure

Materials

Au, Ag, Cu, and Ni polycrystalline (99.9999%) substrates, glassy carbon substrates, and SUS 316L substrates for the respective working electrodes for the electrochemical measurements were acquired from Nilaco Corporation. Polycrystalline Ag and Cu, and SUS 316L foams (Model MF-40), for potential step chronoamperometry (PSC), *in situ* diffuse reflectance infrared Fourier transform spectroscopy (DRIFTS), conventional Raman spectroscopy, and surface enhanced Raman scattering (SERS) were purchased from Nagamine Manufacturing Co., Ltd.

Polyvinylferrocene (PVFc) and multi-walled CNT (MWCNT) (L = 6 ~ 13 nm × 2.5 ~ 20 µm), constituent materials for the counter electrode were obtained from Polysciences Inc. and Sigma-Aldrich, respectively. Gas diffusion layers, JNT20, used as counter electrode substrates, were purchased from JNTC. N-methylpyrrolidone (NMP), the solvent to dissolve PVFc, was obtained from Tokyo Chemical Industry Co., Ltd. Whatman-2 filter papers were purchased from General Electric- Health.

Trimethylpropylammonium bis (trifluoromethanesulfonyl) imide ([$TMPA^+$][$TFSI^-$]), for use as the electrolyte, was acquired from Tokyo Chemical Industry Co., Ltd.

The gas mixtures, CO_2, N_2, and synthetic air (400 ppm CO_2, 21% O_2 and 79% N_2) and synthetic air without CO_2 (21% O_2 and 79% N_2), for use in the electrolysis experiments, were purchased from Tomoe Shokai Co., Ltd.

The other compounds, such as KCl, which was used for the electrochemical roughening of Ag foam, and sodium oxalate, as the standard material for the titration of the ionic liquid, were acquired from Fujifilm Wako Pure Chemical.

Apparatus

DRIFT spectra were recorded using a Thermo Fisher Scientific Nicolet iS50 FT-IR spectrometer. Gas chromatography with a thermal conductivity detector was carried out using an Agilent Technologies 7890A instrument with an Agilent Inc. TC-Molsieve 5A column. Ion chromatography was performed using a Shimadzu Prominence HIC-SP instrument with a Shim-pack IC-SA2 column. X-Ray photoelectron and Auger spectra were recorded using an ULVAC-PHI PHI 5000 VersaProbe II system with Al Kα radiation. X-ray diffraction (XRD) patterns were acquired using a Rigaku SmartLab system at 298 K using Cu Kα radiation. Conventional Raman spectroscopy and SERS were carried out at room temperature using a RENISHAW inVia Raman microscope with a 10 × objective and an excitation radiation wavelength of 785 nm. Scanning electron microscopy (SEM) for the surface analyses of the metal foams was performed using a JEOL JSM-7800F Prime equipped with Thermo Fischer Scientific Energy Dispersive X-ray Spectroscopy (EDS) operated in backscattered detector mode (20 kV). The sample was mounted with double-sided carbon tape. Cross-sectional SEM of the SUS 316L foam was carried out using a ZEISS XVision200TB instrument (3 kV). In preparation for this analysis, the SUS 316L foam was subjected to focused ion beam (FIB) milling using SII nanotechnology XVision200TB (30 kV). Scanning transmission electron microscopy (STEM) and energy dispersive X-ray spectroscopy (EDS) for the cross-section analysis was performed employing JEOL JEM-ARM200F (200 kV) and JEOL silicon drift detector, respectively. Karl Fischer titration of the IL, [$TMPA^+$][$TFSI^-$], was measured using Nittoseiko Analytech CA-200 equipment using AQUAMICRON AX and AQUAMICRON CXU as the electrolytes. The CO_2 concentration in the custom-built closed reaction system was monitored using a SwitchScience S-300L-3V gas sensor calibrated by synthetic air and gas chromatography with a thermal conductivity detector.

Preparation of metal, glassy carbon electrodes for electrochemical measurements

Au, Ag, Cu, Ni, and SUS 316L samples for CV measurements were prepared from 0.1 mm-thick polycrystalline foil (Nilaco, 99.9999 %). The surface of the samples was prepared by using 0.05 mmφ alumina for about 10 min and subsequently cleaned with Milli-Q water for 30 min. The samples were subsequently chemically washed in an acidic solution, 1.0 M HCl or 1.0 M H_2SO_4, followed by ultrasonic cleaning in Milli-Q water for 5 min. The Cu and SUS 316L foams for PSC were first washed with 1.0 M HCl and subsequently cleaned using only Milli-Q water in the ultrasonic bath. The Ag foam for PSC was washed with 1.0 M H_2SO_4, followed by immersion into Milli-Q water with ultrasonication.

Preparation of PVFc/MWCNT counter electrode for PSC

The counter electrodes modified with PVFc were prepared according to the previously established procedure. The composite was prepared as follows: a suspension of 500 mg of PVFc in 150 mL of NMP was ultrasonicated at 5 °C for 20 min, followed by the addition of 1 g MWCNT to the polymer suspension and sonication for 20 min to form the PVFc/MWCNT ink. Then, the PVFc/MWCNT ink was spread over the gas diffusion layer (GDL) substrate (50 mm × 50 mm), dried at 120 °C for 2 h, and finally dried under vacuum at room temperature, overnight.

Preparation of roughened Ag electrode for in *situ* SERS measurements

The roughened Ag electrode was prepared according to the previously reported procedure. First, the Ag foam was ultrasonically washed with Milli-Q water. Then, the Ag foam was electrochemically cycled for five oxidation-reduction cycles in an aqueous solution of 0.2 M KCl from −0.31 V to + 0.39 V vs. Ag/AgCl. Finally, the potential was held at the cathodic vertex before the roughened Ag foam was removed from the solution and rinsed thoroughly with Milli-Q water.

Preparation of the sample for cross-section STEM analysis

The SUS 316L foam for the cross-sectional STEM analysis was loaded into the FIB system and a carbon film was deposited on the surface (1 µm). Subsequently, the sample was milled by FIB (30 kV).

Electrochemical cell assembly

Electrochemical cells were assembled by arranging the components in the following order (from the top window to the bottom substrate): Metal foam; IL; electrolyte separator; IL; PVFc/MWCNT-coated GDL. The electrolyte separators were Whatman-2 cellulose filter paper and the IL was [$TMPA^+$][$TFSI^-$].

Electrochemistry

CV measurements were performed using a Solartron Analytical ModuLab XM analyzer, using pure metal substrates, glassy carbon, or the SUS 316L substrate as the working electrode, Pt wire as the counter electrode,

and $Ag/AgNO_3$ as the reference electrode. The CV measurements were conducted in the potential range of 0.0 V ~ –1.5V vs. $Ag/AgNO_3$ at a sweep rate of 10 mV/s. The reference electrode was formed with two layers of glass tube to prevent the electrolyte or other electrodes from being contaminated with Ag. The IL, $[TMPA^+][TFSI^-]$, was used as the electrolyte. The use of PSC to measure the CO_2 concentration and record the *in situ* DRIFT spectra is described in the next subsection.

Monitoring the CO_2 concentration and recording *in situ* DRIFT spectra during PSC

The CO_2 concentration was measured and *in situ* DRIFT spectra were recorded during PSC experiments in the custom-built ***atmosphere control electrochemical measuring system (ACEMS)***. The design of this system is described in the results section. *In situ* DRIFTS measurements were carried out with a Thermo Fisher Scientific Nicolet iS50 FT-IR spectrometer equipped with a HgCdTe (MCT) detector. Electrochemical measurements were performed using the Solartron Analytical ModuLab XM analyzer with Ag, Cu, or SUS 316L foam as the working electrode and PVFc/MWCNT as both the counter and reference electrodes. The IL, $[TMPA^+][TFSI^-]$, was used as the electrolyte and either 400 ppm CO_2/N_2 (400 ppm CO_2 and 99.96% N_2) or synthetic air (400 ppm CO_2, 21% O_2, and 79% N_2) were used as the gases in the ***ACEMS*** reactor. The electrochemical cell was assembled as described above, after which the atmosphere in the ***ACEMS*** was replaced with the aforementioned reaction gases. Accurate measurement of the CO_2 concentration during the PSC experiments required the CO_2 concentration to be stabilized until it remained constant before the experiments. The DRIFTS measurements were performed in combination with PSC at the following potentials: –1.5 V vs. C.E., 1500 s; 0.0 V vs. C.E., 500 s; 1.0 V vs. C.E., 1000 s on the basis of the spectrum measured at 0 s as the background. The spectral domain was 4000–1000 cm^{-1} (resolution 4 cm^{-1}, 32 scans). These electrodes were used to record at least three measurements to confirm their reproducibility.

In situ Raman and SERS measurements

In situ Raman and SERS spectra were recorded with a RENISHAW inVia Raman microscope, and the electrochemical reaction was controlled by the same electrochemical analyzer used for CV and DRIFTS measurements. The series of measurements was carried out using Ag or roughened Ag foams as the working electrode in the ***ACEMS*** in an atmosphere of synthetic air. The counter electrode and electrolyte used for the measurements were the same as those employed for the DRIFTS measurements. Measurements were performed both without and with an applied potential (–1.5 V vs. C.E.).

Measurements of oxalate in ionic liquid

The IL from the electrochemical cell used for PSC was collected by removing the IL (1 mL) drop wise for subsequent analysis. The collected IL was added to Milli-Q water (5 mL), which was subsequently shaken to conduct liquid-liquid extraction. The oxalate migrated to the aqueous solution, which was analyzed by ion chromatography. The oxalate was extracted for both the used and unused electrochemical cells. A standard oxalate solution, prepared using sodium oxalate, was also measured by ion chromatography to obtain a calibration curve.

Results and Discussion

CV measurements with metal and glassy carbon electrodes

The metal electrodes (Au, Ag, Cu, Ni, and SUS 316L) for the CV measurements were characterized by X-ray diffraction (XRD) and X-Ray photoelectron spectroscopy (XPS). The metal electrodes (Ag, Cu, and SUS 316L foams) used in the PSC experiments were also characterized by XRD, XPS, and scanning electron microscopy (SEM). The XRD measurements of the electrodes and foams confirmed that Ag, Cu, and SUS 316L were not oxidized and were polycrystalline in the bulk phase. The numerous well-resolved peaks on the XRD pattern of SUS 316L correspond to austenite. The XPS and SEM analyses indicate that SUS 316L consists of Fe, Cr, Ni, and Mo, in good agreement with previous studies[23]. Cross-sectional scanning transmission electron microscopy (STEM) revealed that from the surface to a depth of 10 nm, SUS 316L mainly consisted of iron oxide, thereby confirming the XPS results.

CV measurements were performed by employing the metal and glassy carbon electrodes to examine the response of each electrode to the gases generated during the electrochemical reaction. The IL, trimethylpropylammonium bis (trifluoromethanesulfonyl) imide ($[TMPA^+][TFSI^-]$), was chosen as the electrolyte for two reasons: 1) contrary to imidazolium-type ILs, $[TMPA^+][TFSI^-]$ does not tend to be electrochemically reduced at negative potentials because it does not have an aromatic ring structure[24]; 2) the IR spectrum of $[TMPA^+][TFSI^-]$ does not overlap with those of the intermediates produced during electrochemical CO_2 reduction, which are generally in the range 1350–1800 cm^{-1}[25]. In this study, the water concentration in the IL, measured by Karl Fischer titration, was approximately 0.063%. The CV measurements were conducted in 100% CO_2, a gas mixture without CO_2 (21% O_2 and 79% N_2), and a gas mixture containing 50% CO_2 (50% CO_2, 10% O_2 and 40% N_2) as the atmosphere. Synthetic air (400 ppm CO_2, 21% O_2 and 79% N_2) was not used in the CV measurements because of its ambiguous response to trace amounts of CO_2 in the atmospheric gas. In the mixed gas atmosphere, redox waves of O_2 were observed for the Au, Ag, Cu, and glassy carbon electrodes as previously reported[13,26-28], whereas the redox wave was obscure for the SUS 316L electrode. For the Ni electrode, the weak reduction current corresponding to O_2 reflected its inertness against O_2. In the atmosphere of mixed gas containing 50% CO_2, the oxidation waves of all the electrodes disappeared (Au, Ag, Cu, and glassy carbon)[12,13] and, interestingly, the potential of the O_2 reduction wave shifted to the positive side for the SUS 316L electrode. According to previous studies[12,13], the disappearance of the oxidation waves for the electrodes in the atmosphere containing both O_2 and CO_2 is attributed to the preferred generation of $O_2^{\bullet-}$ when O_2 is reduced at negative potentials to enable CO_2 to react continuously to irreversibly form products such as carbonate[17,19,29], peroxydicarbonate[12,13,15,16], or oxalate[19,20]. In other words, the CO_2 reduction reactivity is dependent on the electrochemical catalytic activity of each metal against O_2. The greater importance of O_2 reduction is also implied in comparison to the result of the CV measurements under CO_2 atmosphere, in which smaller reduction currents were measured than those observed in the mixed gas atmosphere. The reactivity of each metal electrode against O_2 was previously examined using density functional theory (DFT) calculations[30-33] to create a volcano plot of the reactivity vs. oxygen adsorption energy. In view thereof, to conduct a more in-depth study of the electrochemical CO^2 reduction mechanism in combination with O_2, we chose three representative substrates, Ag, Cu, and SUS 316L, which reportedly strongly repel, moderately repel, and readily adsorb oxygen, respectively[30-33]. As confirmed by XPS and cross-sectional STEM, the surface of SUS 316L consists of iron oxide, for which the adsorption energy for O_2 is high at –130 kJ/mol (–1.35 eV)[34],

which implies that SUS 316L tends to adsorb oxygen. Previous investigations of the electrochemical reduction of CO_2 and O_2 in aprotic solution[12-17,19,20,29] proposed a few reaction pathways. Representative thereof is the generation of peroxydicarbonate, reported by Halilu et al., who suggested that sequential reactions are more plausible than a one-pot reaction[12]:

(1) generation of peroxydicarbonate
(Maximum of theoretical electron utilization rate = 100%)
1) sequential reactions
$O_2 + e^- \leftrightarrow O_2^{\bullet-}$: −0.92 V vs. $Ag/AgNO_3$
$O_2^{\bullet-} + CO_2 \rightarrow CO_4^{\bullet-}$
$CO_4^{\bullet-} + CO_2 \rightarrow C_2O_6^{\bullet-}$
$C_2O_6^{\bullet-} + O_2^{\bullet-} \rightarrow C_2O_6^{2-} + O_2$
2) one-pot reaction
$O_2 + 2CO_2 + 2e^- \leftrightarrow C_2O_6^{2-}$: −0.22 V vs. $Ag/AgNO_3$

The maximum theoretical electron utilization rate is calculated by the ratio between the number of CO_2 molecules and the number of electrons in the equations. The peroxydicarbonate was identified by FT-IR or Raman measurements[13-17,19,35]. In many cases, the formation of peroxydicarbonate reportedly proceeded on carbon or Au electrodes, both of which are categorized as repulsive of oxygen[13,16,17,19].

Additionally, the formation of carbonate was investigated[17,19,29], also by assuming the reaction to be sequential:

(2) generation of carbonate
(Maximum of theoretical electron utilization rate = 50%)
1) sequential reaction
$O_2 + e^- \leftrightarrow O_2^{\bullet-}$: −0.92 V vs. $Ag/AgNO_3$
$O_2^{\bullet-} + CO_2 \rightarrow CO_4^{\bullet-}$
$CO_4^{\bullet-} + CO_2 \rightarrow C_2O_6^{\bullet-}$
$C_2O_6^{\bullet-} + O_2^{\bullet-} \rightarrow C_2O_6^{2-} + O_2$
$C_2O_6^{2-} + 2O_2^{\bullet-} \rightarrow 2CO_3^{2-} + 2O_2$
2) one-pot reaction
$O_2 + 2CO_2 + 4e^- \leftrightarrow 2CO_3^{2-}$: 0.28 V vs. $Ag/AgNO_3$

Similar to the peroxydicarbonate production, the electrode on which the electrochemical CO_2 reduction reaction proceeds to produce carbonate often consisted of carbon materials[17,19,29]. .Although metal electrodes for Li-CO_2 batteries were also investigated[36], the metals were principally used as catalyst for the decomposition of carbonate. Carbonate is considered an undesirable product of the electrochemical reduction of CO_2 because of its low theoretical electron utilization rate (50%) and high decomposition overpotential[6,16-21,36].

In comparison to peroxydicarbonate or carbonate[19,20], few reports of the production of oxalate from the electrochemical reduction of CO_2 in the presence of O_2 have appeared, although the generation of oxalate is frequently researched in studies concerned with the electrochemical reduction of CO_2 in the absence of other gases in aprotic solution on Pb, SUS 304L, Mo_2C, or Hg electrodes[9,37-39]. Sadat et al. studied the electrochemical reduction of CO_2 in coexistence with O_2, demonstrated the generation of aluminum oxalate ($Al_2(C_2O_4)_3$) on the stainless steel (SUS) electrode[20]:

(3) generation of oxalate
(Maximum of theoretical electron utilization rate = 100 %)
1) sequential reaction
$O_2 + e^- \leftrightarrow O_2^{\bullet-}$: −0.92 V vs. $Ag/AgNO_3$
$O_2^{\bullet-} + CO_2 \rightarrow CO_4^{\bullet-}$
$CO_4^{\bullet-} + O_2^{\bullet-} \rightarrow CO_4^{2-} + O_2$
$CO_4^{2-} + CO_2 \rightarrow C_2O_4^{2-} + O_2$

O_2 seems to play the role of an electron mediator via $O_2^{\bullet-}$ in this series of reactions; however, the mechanism whereby CO_2 and O_2 are electrochemically reduced is still unclear due to the complex reduction reaction pathways, as in the above equations. Thus, we decided to perform in situ diffuse reflectance infrared Fourier transform spectroscopy (DRIFTS) measurements to monitor the CO_2 concentration under PSC using the ***atmosphere control electrochemical measuring system (ACEMS)***. In the measurements, we employed three metal electrodes, Ag, Cu and SUS 316L in view of the different catalytic behaviors suggested previously[12,13,30-33].

In situ spectroscopic measurements to monitor CO_2 with *ACEMS*

(i) Design of ACEMS

We designed ***ACEMS*** (Fig. 1) to i) perform electrochemical analyses such as PSC, ii) monitor changes in the CO_2 concentration in a sealed environment, and iii) perform in situ spectroscopic measurements such as DRIFTS or Raman. Hence, the system has two components, an electrochemical device, and a sealed container with electric wiring. The electrochemical device, an assembled electrochemical cell (described in the Experimental Procedure section of Supporting Information) is sandwiched between a lid and a base, both of which are conductive. The working electrode of the cell is attached to the lid and the counter electrode is located on the base. The lid has two types of slits: 32 small circular holes to allow the gas to pass through, and an elongated slit as an optical path for infrared or nm lasers Fig. 1b and Fig. 1e). The electrochemical instrument is mounted inside and electrically connected with the sealed container. Other than electric wiring, the sealed container accommodates the CO_2 sensor, gas exchange pipes, and an optical quartz window (Fig. 1a). To enable ***ACEMS*** to be used in spectroscopic measurements, the thickness of the quartz window and distance between the window and lid of the electrochemical instrument were designed as 1.0 mm and 0.5 mm, respectively (Fig. 1c).

To determine the reaction potential of the working electrode in ***ACEMS***, we first performed CV measurements in a glass cell using the polyvinylferrocene (PVFc)/multi-walled CNT (MWCNT) electrode, abbreviated as PVFc/MWCNT, as the counter electrode (C.E.) in ***ACEMS***. Although the reduction/oxidation potentials differed widely, the redox potential of PVFc/MWCNT was estimated as 0.15 V vs. $Ag/AgNO_3$. PSC experiments were performed under the respective gas atmosphere in the following potential steps for the working electrode: first step: −1.5 V vs. PVFc/MWCNT as C.E./1500 seconds; second step: 0.0 V vs. C.E./500 seconds, final step: 1.0 V vs. C.E./1000 seconds. This PSC cycle was repeated three times for each experiment. Fig. 2 and Fig. 3 show the CO_2 concentrations and DRIFT spectra for the Ag, Cu, or SUS 316L electrodes in 400 ppm CO_2/N_2 (400 ppm CO_2 and 99.96% N_2) and in synthetic air (400 ppm CO_2, 21% O_2, and 79% N_2). As in the CV measurements, the aprotic IL, [$TMPA^+$][$TFSI^-$], was also employed as electrolyte.

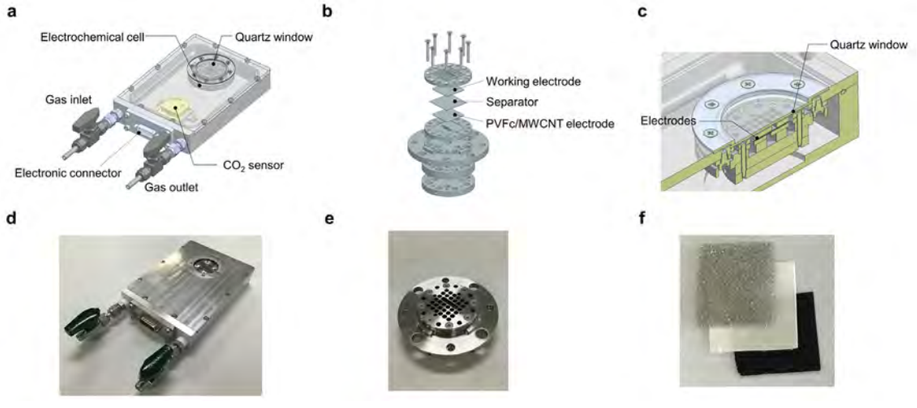

Fig. 1 Schematic illustrations and photographs of the atmosphere controlled electrochemical measuring system (*ACEMS*). Schematics of (a) *ACEMS* with the electronic connector, CO_2 sensor, quartz window and gas inlet/outlet tubes; (b) electrochemical device; (c) cross-section of *ACEMS*. Photographs of (d) *ACEMS* (sealed); (e) the electrochemical device and (f) the electrochemical cell: metal foam; electrolyte separator; PVFc/MWCNT-coated GDL

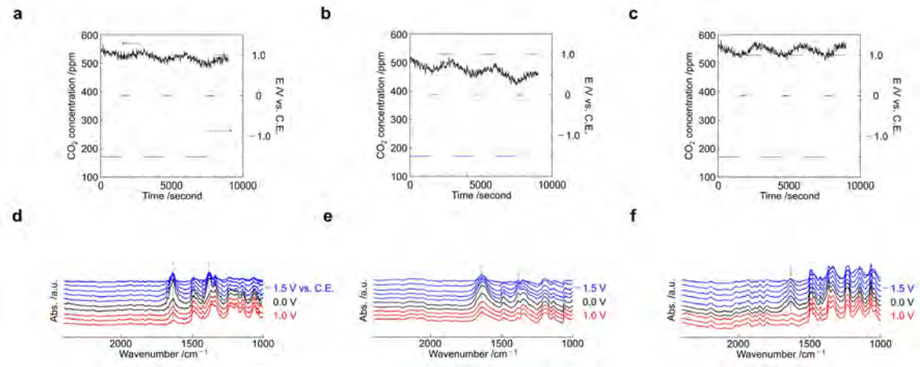

Fig. 2 Changes in the CO_2 concentration and DRIFT spectra through electrochemical reactions in *ACEMS* under 400 ppm CO_2/N_2. (a), (b) and (c) changes in the CO_2 concentration; (d), (e) and (f) DRIFT spectra using Ag, Cu, and SUS 316L electrodes, respectively

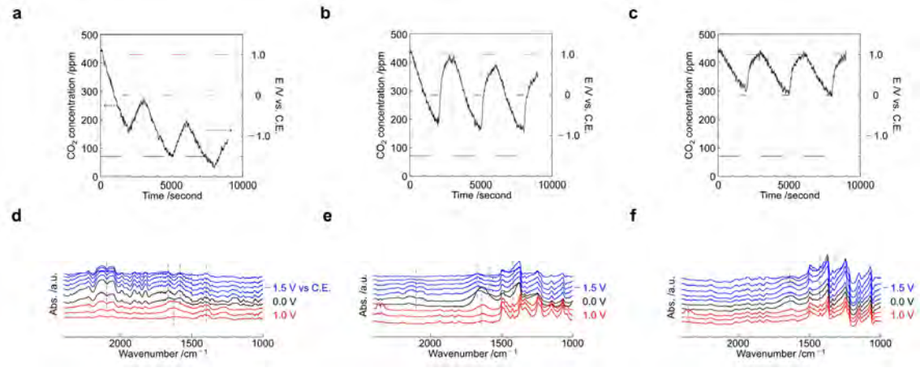

Fig. 3 Changes in the CO_2 concentration and DRIFT spectra during electrochemical reactions in *ACEMS* under an atmosphere of synthetic air. (a),(b) and (c) variation of the CO_2 concentration; (d),(e) and (f) DRIFT spectra using Ag, Cu, and SUS 316L electrodes, respectively

(ii) DRIFTS measurements in 400 ppm CO_2/N_2

The measurements in 400 ppm CO_2/N_2 gave rise to weak reduction currents at an applied potential of −1.5 V and the changes in the CO_2 concentration in ***ACEMS*** were trivial for each respective electrode (Fig. 2). Although the variations in the CO_2 concentration were also very small, we were interested in whether they increased/decreased in comparison with the DRIFTS results.

For the Ag electrode, the CO_2 concentration decreased slightly during three PSC cycles, suggesting that an irreversible reaction proceeded in the aprotic ionic liquid at applied potentials between −1.5 V and 1.0 V (Fig. 2a). Previously, Xie et al. showed that the electrochemical reduction of CO_2 in an aprotic solution using a Zn electrode[8] occurs via disproportionation:

(4) disproportionation of CO_2

$$2CO_2 + 2e^- \rightarrow CO + CO_3^{2-} : -1.02 \text{ V vs. } Ag/AgNO_3$$

We postulate that the same disproportionation reaction occurred in our experiment because, with the Ag electrode, the electrochemical reduction of CO_2 in aprotic solutions purportedly produces CO[9]. Moreover, CO, as the product of the reduction reaction supposedly easily diffuses offshore into the ionic liquid or gas phase from the electrode surface. As a result, the only reactant for oxidation at 1.0 V in PSC cycles is presumably carbonate, and the amount of CO_2 produced in the following equation is estimated to be smaller than that in the reduction reaction at negative potential:

(5) oxidation of carbonate

$$2CO_3^{2-} \rightarrow 2CO_2 + O_2 + 4e^- : 0.28 \text{ V vs. } Ag/AgNO_3$$

The DRIFTS measurements using the Ag electrode (Fig. 2d) show peaks at 1380 and 1640 cm^{-1} at −1.5 V, which implies that they are attributable to products of the electrochemical CO_2 reduction. The other observed peaks, at 1060, 1140, 1200, 1350, and 1480 cm^{-1} were previously ascribed to $[TMPA^+][TFSI^-]$[25]. The assignment of the peaks at 1380 and 1640 cm^{-1} using the Ag electrode does not seem to have been reported before; however, the peaks were assigned to carbonate because FT-IR bands with the same characteristics were reported by other groups using a Cu electrode in organic solutions[40] and similar peaks were detected by the Cu electrode used in our DRIFTS measurement. We assigned the peaks at 1380 and 1640 cm^{-1} to the C–O and C=O stretching vibrations of carbonate, respectively[40] (details in Table 1). Unfortunately, ascription of the peak at 1640 cm^{-1} is difficult because other candidates such as oxalate or peroxydicarbonate are also detected in the same IR region[14,15,17,19,38,42]. Subramanian et al. previously reported that oxalate was produced on the SUS 304L electrode, as confirmed by FT-IR measurements[37]. In their study, they assigned the FT-IR peaks at 1320, 1363, and 1645 cm^{-1} to the CO_2^-, C–C, and C=O stretching vibrations of oxalate, respectively. Wu et al. also ascribed the peaks at 1327 and 1645 cm^{-1} to oxalate[38]. In all related research[19,37,38,41], the oxalate peak at low IR wavenumbers is generally detected in the range 1320–1370 cm^{-1}, which indicates that the peak at 1380 cm^{-1} in our DRIFTS measurements using the Ag electrode is not attributable to oxalate. Although peroxydicarbonate is also supposedly generated, based on the ascriptions of peaks reportedly observed at 1260–1360 and 1630–1750 cm^{-1}[13-17,19,35], this compound can be excluded from the candidate products of the electrochemical reaction on the Ag electrode under 400 ppm CO_2/N_2, because O_2 is required to produce peroxydicarbonate from CO_2 (Equation (2)). Therefore, in the DRIFTS measurements without O_2 in the atmosphere, the peaks observed for the Ag electrode at negative potential can reasonably be ascribed to carbonate following Equation (4). We unfortunately could not discern CO as another product of the disproportionation of CO_2 in the measurements, possibly due to CO diffusion into the electrolyte and/or gas phase, as mentioned above. Adjustment of the applied potential to a positive value enabled the two peaks attenuated at 1380 and 1640 cm^{-1} to be observed, indicating that the carbonate was oxidized in accordance with Equation (5).

For the Cu electrode, the changes in the CO_2 concentration and IR bands were similar to those with the Ag electrode (Fig. 2b and Fig. 2e). The only slight difference between the evaluations using the Cu and Ag electrodes is the peaks ascribed to CO around 2000–2200 cm^{-1} for the Cu electrode in DRIFTS measurements[42]. In both cases, the disproportionation of CO_2 to generate CO and carbonate occurs on both electrodes according to Equation (4). Table 1 presents a detailed assignment of the peaks attributed to carbonate in our DRFITS measurements.

With the SUS 316L electrode, although the CO_2 concentration changed negligibly during the PSC cycles, similar to the observations with the other electrodes, this electrode produced different results in the DRIFTS measurements (Fig. 2c and Fig. 2f). The peak at 1380 cm^{-1}, observed for the Ag or Cu electrodes at negative potential, was not detected for

Table 1 Assignment of peaks observed in DRIFTS measurements employing the Au, Cu, or SUS 316L electrodes under 400 ppm CO_2/N_2 atmosphere

Electrode	Applied Potential /V vs. C.E.	Wavenumber /cm^{-1}		Assignment	Reference
		This study	Previous studies		
Ag	−1.5	1380	1364~1388	C−O stretching of CO_3^{2-}	40
	−1.5	1640	1646	C=O stretching of CO_3^{2-}	40
Cu	−1.5	1380	1364~1388	C−O stretching of CO_3^{2-}	40
	−1.5	1640	1646	C=O stretching of CO_3^{2-}	40
	−1.5	2000~2200	2138	C−O stretching of CO	42
SUS 316L	−1.5	1640	1645	C=O stretching of $C_2O_4^{2-}$	19,37,38,41
	1.0	2300~2400	2341	C=O stretching of CO_2	42

the SUS 316L electrode. As mentioned above, the peak at 1350 cm^{-1}, which is close to the IR band at 1380 cm^{-1}, is attributed to [TMPA$^+$][TFSI$^-$]. Other than the [TMPA$^+$][TFSI$^-$] peaks, the only other prominent peak was at 1640 cm^{-1}. Similar to the results using the Ag or Cu electrodes, the peak at 1640 cm^{-1} de-intensified upon changing to a positive potential, suggesting that it was generated from the electrochemical reduction of CO_2. We assigned the peak based on previous studies using the SUS 304L electrode[19,37,41], especially that by Subramanian et al. That is, the peak at 1640 cm^{-1} is assignable to the C=O stretching vibration of oxalate. The peak at 1320–1370 cm^{-1}, the frequency of the stretching vibration of C–O in oxalate was not detected because of the overlap of [TMPA$^+$][TFSI$^-$] frequencies. Table 1 presents a detailed assignment of the peaks observed in our DRIFTS measurements using the SUS 316L electrode. Oxalate generation on the SUS 316L electrode in these measurements was confirmed by ion chromatography. Interestingly, DRIFTS measurements employing the SUS 316L electrode at positive potential enabled CO_2 production to be affirmed, based on the peak at 2300~2400 cm^{-1}[42]. As indicated by changes in the CO_2 concentration, which is comparatively reversible by varying the potential between negative and positive, the reaction on the SUS 316L electrode is reversible, presumably according to following reaction:

(6) reversible reaction between CO_2 and oxalate

$2CO_2 + 2e^- \leftrightarrow C_2O_4^{2-}$: −0.42 V vs. Ag/$AgNO_3$

In addition, the reversibility of the CO_2 concentration through PSC cycles using the SUS 316L electrode suggests that the electrolysis of CO_2 does not generate diffusion products such as CO gas.

(iii) DRIFTS measurements in synthetic air

The evaluation under an atmosphere of synthetic air revealed drastic differences, both in the CO_2 concentration and DRIFT spectra, in comparison to those in 400 ppm CO_2/N_2 (Fig. 2 and Fig. 3). The reaction currents were stronger and changes in the CO_2 concentration in ***ACEMS*** were larger than those measured in an atmosphere devoid of O_2. Although O_2 presumably promotes the electrochemical reduction of CO_2[18,43], this is the first confirmation of the effect of O_2 on the reduction of CO_2 using both CO_2 gas analysis and in situ spectroscopy.

For the Ag electrode, the CO_2 concentration in *ACEMS* decreased stepwise according to the PSC cycles, similar to that in 400 ppm CO_2/N_2, indicating that the reaction is irreversible (Fig. 3a). In addition, the DRIFT spectra revealed the production of CO, evident from the peaks around 2000~2200 cm^{-1} at −1.5 V (Fig. 3d). We presumed that CO_2 underwent disproportionation on the Ag electrode regardless of the presence of O_2 under the evaluation conditions. Interestingly, CO production in the reduction reaction in synthetic air seems to be more intensive than that under 400 ppm CO_2/N_2, as confirmed by GC analysis. Carbonate, another product in the disproportionation of CO_2, was not observed by DRIFTS at negative potential, possibly because it is shielded by CO gas in the optical path. When the potential was changed to positive, the CO_2 peaks around 2300~2400 cm^{-1} were not detected for the Ag electrode unlike for the other electrodes (Fig. 3d, Fig. 3e and Fig. 3f)[42], suggesting that the reactions on the Ag electrode during PSC cycling are irreversible. Additionally, the small doublet around 1500~1700 cm^{-1} and singlet at 1400 cm^{-1} were ascribed to asymmetric peroxydicarbonate ($^-$OOC(=O)OC(=O)O$^-$). We inferred that CO and carbonate were produced via the asymmetric peroxydicarbonate intermediate of the electrochemical reduction of CO_2 and O_2 (this is discussed in more detail later). Even though aarbonate was not observed at negative potential, it was identified as a peak near 1650 cm^{-1} by applying a positive potential[40] because it is an anionic species that tends to approach the positively charged electrode[44]. In addition, carbonate was assumed to diffuse offshore into the ionic liquid via a reduction reaction. These observations confirmed that the disproportionation of CO_2 on the Ag electrode certainly occurred at −1.5 V.

For the Cu and SUS 316L electrodes, the CO_2 concentration underwent similar changes (Fig. 3b and Fig. 3c). However, DRIFTS measurements with the Cu electrode revealed a slight decrease in the CO_2 concentration in the course of the PSC experiments and a minor CO peak around 2000~2200 cm^{-1} (Fig. 3b and Fig. 3e). These results suggested the partial disproportionation of CO_2 at negative potential. In addition to this CO peak, another peak was detected near 1670 cm^{-1} at −1.5 V with the Cu electrode (Fig. 3e). A small shoulder peak also appeared near 1600 cm^{-1} to form a pair with the peak at 1670 cm^{-1}. This pair of peaks resembles the peaks observed in the same IR region with DRIFTS measurements using the Ag electrode in synthetic air. When the applied potential was changed to 0.0 V, the peak near 1670 cm^{-1} underwent redshift to 1640 cm^{-1} and was simultaneously intensified. However, the peak near 1640 cm^{-1} disappeared and a new peak attributed to CO_2 appeared instead at 2300~2400 cm^{-1} by switching to a positive potential. DRIFTS measurements are highly sensitive to chemical species that are densely present on the substrate surface[45]. Additionally, the chemical species on the electrodes changed depending on the applied potential. This led us to infer that the peaks observed around 1600~1670 cm^{-1} at −1.5 V are different from those at 0.0 V. As mentioned above, the peaks around 1600~1670 cm^{-1} can be attributed to carbonate, oxalate, or peroxydicarbonate. Considering the IR bands around 1400 cm^{-1}, a shoulder peak appeared in the negative potential range to 0.0 V, but disappeared at the positive potential. Because the peaks that are enhanced at negative potential or 0.0 V are not attributed to oxalate in the above assignments (Table 1), they can be ascribed to either carbonate or peroxydicarbonate. The assignments of the peaks observed in the DRIFTS measurements using the Cu electrode are discussed in detail later.

DRIFTS measurements using the SUS 316L electrode revealed a peak at 1640 cm^{-1} and a shoulder peak at 1400 cm^{-1} at negative potential, and they persistently remained when the potential was changed from −1.5 V to 0.0 V (Fig. 3f). The potential-dependent spectral behavior using the SUS 316L electrode differs from that using the Cu electrode. The peaks at 1400 and 1640 cm^{-1} vanished at 1.0 V, and were replaced by a new peak attributed to CO_2 that appeared around 2300~2400 cm^{-1}. Based thereupon, the products of electrochemical reduction of CO_2 and O_2 on SUS 316L were also presumed to be either carbonate or

Table 2 Summary of products on each electrode in the electrochemical reduction of CO_2 with/without O_2

Electrode	Products from 400 ppm CO_2 at −1.5 V vs. C.E.	
	Without O_2	With O_2
Ag	CO, CO_3^{2-}	CO, CO_3^{2-}
Cu	CO, CO_3^{2-}	CO_3^{2-}
SUS 316L	$C_2O_4^{2-}$	$C_2O_6^{2-}$

peroxydicarbonate, similar to the case using the Cu electrode. The only slight difference between the SUS 316L and Cu electrodes was that the IR bands were not affected at negative potential (between −1.5 V and 0.0 V).

Although reversible reactions as those in Equation (1) or (2) were inferred from our results, the products generated in the electrochemical reduction of CO_2 and O_2 at negative potential on the Cu or SUS 316L electrodes were inconclusive. Furthermore, the mechanism of CO production on the Ag electrode was not clear in spite of the presence of O_2 in the atmosphere. Thus, we proceeded to examine the mechanism of the electrochemical reduction of CO_2 and O_2 on the three electrodes by evaluating the electron utilization rates for CO_2 capture/release.

(iv) Electron utilization rate as mole of CO_2 per electrons

A valid approach to evaluate the electron utilization rates for CO_2 capture ($\varepsilon_{CO2\text{-}cap.}$) is to use the ratio between the moles of CO_2 reacted and the moles of electrons transferred to determine whether carbonate (maximum of theoretical electron utilization rate = 50 %) or peroxydicarbonate (100 %) is produced on each electrode. Worth noting is that the electron utilization rates are estimable by monitoring the changes in CO_2 concentration and the transferred charge within our ***ACEMS***. The electron utilization rates for CO_2 capture during PSC cycling using the Ag, Cu, or SUS 316L electrodes, 19%, 66%, or 87%, are shown in Fig. 4a as the average of three cycles, respectively. The electron utilization rate for CO_2 capture using the Ag electrode is relatively low compared to that of the other electrodes, indicating that O_2 reduction proceeds excessively and the other reactions involving CO_2 are sluggish. The mechanism of electrochemical CO_2 and O_2 reduction on the Ag electrode is discussed below in more detail based on the Raman results. On the Cu electrode, carbonate is deduced to be a product in the electrochemical reduction of CO_2 and O_2 because the estimated electron utilization rate for CO_2 capture corresponds with the theoretical rate at which carbonate is generated from CO_2 and O_2 (Equation (2)-1)). We also evaluated the electron utilization rates for the release of CO_2 ($\varepsilon_{CO2\text{-}rel.}$) at 1.0 V, that is, mole of CO_2 released per electrons (Fig. 4b). The electron utilization rate for CO_2 release using the Cu electrode is estimated as 52%, suggesting that carbonate is oxidized at 1.0 V according to Equation (2)-2). However, because of the relatively high electron utilization rates for both CO_2 capture and release using the SUS electrode, peroxydicarbonate is presumed as a product from Equation (1). The products on each electrode in the presence/absence of O_2 are summarized in Table 2.

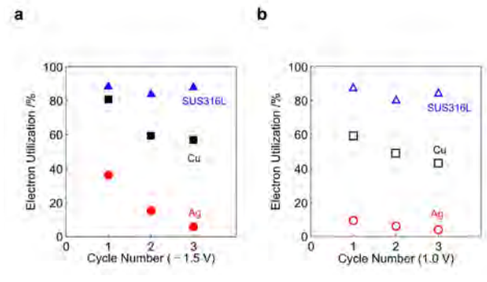

Fig. 4 Estimated electron utilization rates. (a) CO_2 capture ($\varepsilon_{CO2\text{-}cap.}$); (b) CO_2 release ($\varepsilon_{CO2\text{-}rel.}$) in PSC cycles employing the Ag, Cu, or SUS316L electrodes in an atmosphere of synthetic air

Because the reaction pathways of the electrochemical reduction of CO_2 and O_2 on each electrode continued to remain unclear, we performed Raman spectroscopic measurements.

(v) Raman spectroscopy with the Ag electrode

Raman spectroscopy was used to elucidate the mechanism whereby CO_2 is electrochemically reduced on the Ag electrode. With these measurements, we aimed to detect the intermediates that formed during this reaction, not only in the electrolyte but also on the electrode surface. The Raman technique for studying the molecular behavior on the electrode surface during electrochemical reactions is known as surface enhanced Raman scattering (SERS)[28,46,47]. The effect that enables this information to be obtained originates from the surface plasmon resonance of metal nanoparticles such as Ag, Au, or Pt[48]. In other words, a Raman spectrum acquired using a bare metal electrode (rather than nanostructures) contains chemical information about both the electrode surface and the electrolyte at a distance from the electrode. Thus, we prepared two electrodes, bare Ag and roughened Ag, for conventional Raman and SERS spectroscopy, respectively. As described in the Experimental Procedure section of Supporting Information, the roughened Ag was prepared in accordance with a reported procedure[47] and the roughened Ag was characterized using SEM and XPS (Fig. 5b, respectively). The Raman measurements in synthetic air are shown in Fig. 5. Interestingly, peaks ascribed to both symmetric and asymmetric peroxydicarbonates ($^-OC(=O)OOC(=O)O^-$ and $^-OOC(=O)OC(=O)O^-$) were observed in each measurement[15-17,35]. The specific peak assignments are as follows: the peaks at 525, 890, and 1030 cm^{-1} were assigned to the Ag–O stretching vibration of symmetric or asymmetric peroxydicarbonates, the O–O stretching vibration of symmetric peroxydicarbonate, and the O–O stretching vibration of asymmetric peroxydicarbonate, respectively. Other peaks observed around 650~800 cm^{-1} were attributed to IL migrated from the bulk electrolyte to the working electrode at negative potential. The lower intensity of the peak at 890 cm^{-1} than that at 1030 cm^{-1} in conventional Raman spectroscopy implies that the asymmetric form of peroxydicarbonate

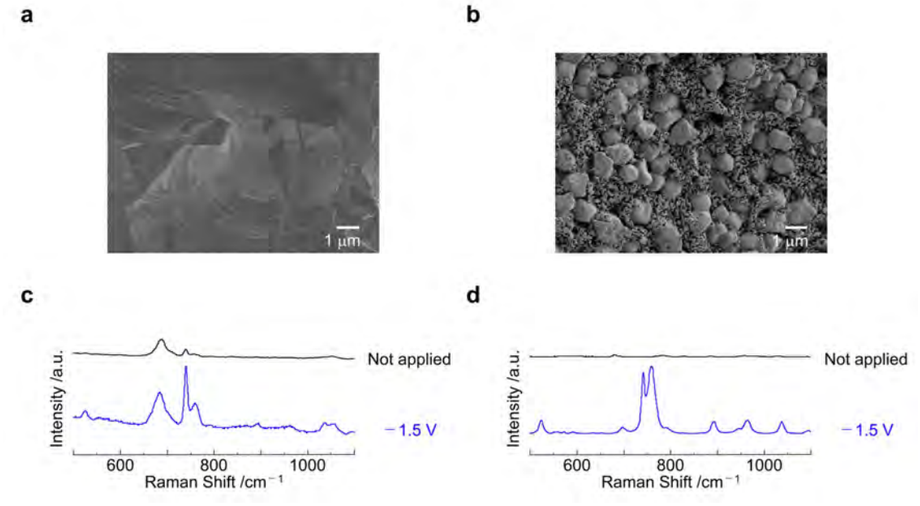

Fig. 5 SEM images, Raman spectra, and SERS measurements of Ag. (a) bare Ag and (b) roughened Ag foams. Spectra acquired by (c) conventional Raman using the bare Ag electrode and (d) SERS measurements using the roughened Ag electrode in an atmosphere of synthetic air

predominantly exists in the bulk electrolyte. The result is in good agreement with that of a previous study on trace-O_2-assisted Li-CO_2 batteries using the in situ SERS technique[17]. Previously[14,17], symmetric and asymmetric peroxydicarbonate was proposed to be generated from CO_2 and $O_2^{\bullet-}$ as follows:

(7) generation of symmetric peroxydicarbonate

$O_2^{\bullet-} + CO_2 \rightarrow {}^{\bullet}OOC(=O)O^-$

${}^{\bullet}OOC(=O)O^- + O_2^{\bullet-} \rightarrow {}^-OOC(=O)O^- + O_2$

${}^-OOC(=O)O^- + CO_2 \rightarrow {}^-OC(=O)OOC(=O)O^-$

(8) generation of asymmetric peroxydicarbonate

$O_2^{\bullet-} + CO_2 \rightarrow {}^{\bullet}OOC(=O)O^-$

${}^{\bullet}OOC(=O)O^- + CO_2 \rightarrow {}^{\bullet}OOC(=O)OC(=O)O^-$

${}^{\bullet}OOC(=O)OC(=O)O^- + O_2^{\bullet-} \rightarrow {}^-OOC(=O)OC(=O)O^- + O_2$

Zhao et al. also studied Li-CO_2 batteries with trace O_2 using both Raman and FT-IR spectroscopy[17]. They reported that reduced O_2 ($O_2^{\bullet-}$) diffuses into the bulk electrolyte because it is highly soluble in the solution, and $O_2^{\bullet-}$ combines with CO_2 in the bulk solution to form asymmetric peroxydicarbonate as a crucial intermediate in the generation of carbonate. In our DRIFTS measurements using the Ag electrode, the small doublet around 1500~1700 cm^{-1} and the singlet at 1400 cm^{-1} (Fig. 3d) correspond well with the IR bands of asymmetric peroxydicarbonate that were previously theoretically calculated[14].

The combined results of our Raman and DRIFTS measurements were analyzed by assuming that the reactions to produce CO and carbonate in the electrochemical reduction of CO_2 and O_2 on the Ag electrode proceed via the asymmetric peroxydicarbonate intermediate:

(9) CO_2/O_2 reduction reaction on Ag electrode

$O_2 + e^- \leftrightarrow O_2^{\bullet-}$: −0.92 V vs. $Ag/AgNO_3$

$O_2^{\bullet-} + CO_2 \rightarrow {}^{\bullet}OOC(=O)O-$

${}^{\bullet}OOC(=O)O^- + CO_2 \rightarrow {}^{\bullet}OOC(=O)OC(=O)O^-$

${}^{\bullet}OOC(=O)OC(=O)O^- + O_2^{\bullet-} \rightarrow {}^-OOC(=O)OC(=O)O^- + O_2$

(in bulk electrolyte)

${}^-OOC(=O)OC(=O)O^- \rightarrow CO + CO_3^{2-} + O_2$

(in bulk electrolyte)

The detailed sequence of reactions that occur on each electrode is presented in Fig. 6a, and the assignments of the FT-IR bands observed in DRIFTS measurements in synthetic air are summarized in Table 3. Although symmetric peroxydicarbonate was observed at 890 cm^{-1} with the SERS measurements (Fig. 5d), the formation of CO and carbonate from symmetric peroxydicarbonate via the dissociation reaction is presumed to be difficult (Fig. 6a). The formation of carbonate in the bulk electrolyte was confirmed by adjusting the potential from negative to 0.0 V in the DRIFTS measurements to reveal a peak near 1640 cm^{-1} that was ascribed to carbonate

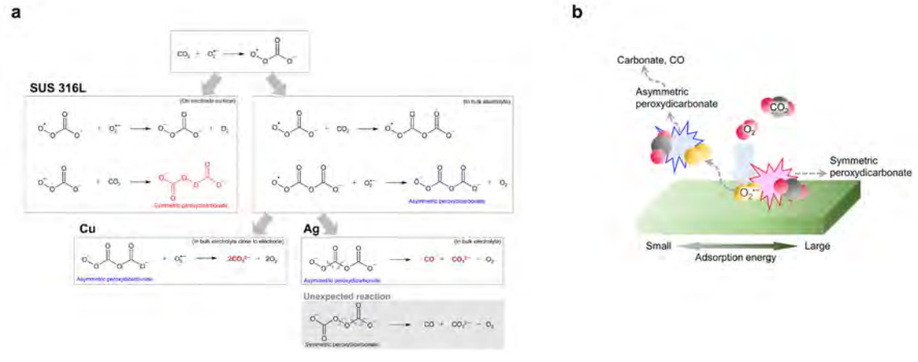

Fig. 6 Reaction pathways and proposed reaction mechanism. Schematic illustrations of (a) reaction pathways on each electrode and (b) plausible reaction mechanism of electrochemical reduction of CO_2 and O_2 to generate different products depending on the type of electrode

Table 3 Assignment of peaks observed in DRIFTS measurements with the Au, Cu, or SUS 316L electrode in an atmosphere of synthetic air

Electrode	Applied potential /V vs. C.E.	Wavenumber /cm^{-1}		Assignment	Reference
		This study	Previous studies		
Ag	−1.5	1500~1700 (d)[a]	1500~1900 (d)[a]	C=O stretching of asymmetric $C_2O_6^{2-}$	14
	−1.5	2000~2200	2138	C−O stretching of CO	42
	1.0	1400	1364~1388	C−O stretching of CO_3^{2-}	40
	1.0	1650	1646	C=O stretching of CO_3^{2-}	40
Cu	−1.5	1600, 1670 (d)[a]	1500~1900 (d)[a]	C=O stretching of asymmetric $C_2O_6^{2-}$	14
	−1.5	2000~2200	2138	C−O stretching of CO	42
	0.0	1400	1364~1388	C−O stretching of CO_3^{2-}	40
	0.0	1640	1646	C=O stretching of CO_3^{2-}	40
	1.0	2300~2400	2341	C=O stretching of CO_2	41
SUS 316L	−1.5	1400	1250	C=O stretching of symmetric $C_2O_6^{2-}$	14,17
	−1.5	1640	1750 (s)	C=O stretching of symmetric $C_2O_6^{2-}$	14,17
	1.0	2300~2400	2341	C=O stretching of CO_2	42

[a] (d) denotes "doublet peak."

adsorbed on the electrode surface (Fig. 3d). The difference between our work and that of Zhao et al. is the absence or presence of Li cations, which promote the formation of carbonate, and led us to speculate that, in our study, the dissociation reaction proceeded owing to the absence of Li cations[17]. Although asymmetric peroxydicarbonate presumably reacts with $O_2^{\bullet-}$ to generate carbonate, as well (Equation (2)), the reaction is limited because $O_2^{\bullet-}$ is prone to diffuse throughout the bulk electrolyte, where it is less likely to encounter asymmetric peroxydicarbonate.

We also delve into the reactions on the Cu or SUS 316L electrodes (Fig. 6a). Unfortunately, we could not acquire sufficient Raman spectra to discuss the mechanism of electrochemical CO_2 and O_2 reduction using the Cu and SUS 316L electrodes. This is attributed to the inadequate enhancement of the Raman signal on these electrodes. Currently, we are attempting to synthesize core/shell nanoparticles for shell-isolated nanoparticle-enhanced Raman spectroscopy (SHINERs) measurements to observe molecular behavior on the electrodes[27,49], which we aim to report in future. Unlike SERS, SHINERs has the advantage of not being limited to noble metal substrates due to core-shell structure of the nanoparticle, which consists of a plasmonic material core such as silver (Ag), gold (Au) and platinum (Pt) and an inert shell such as SiO_2, Al_2O_3, and TiO_2 that inhibits catalytic reaction from the noble metal core. Thus, our mechanistic analysis is based on the results of our CV measurements, DRIFTS measurements, and other analyses. The reaction using the Cu electrode is presumed to proceed as follows:

(10) CO_2/O_2 reduction on the Cu electrode

$O_2 + e^- \leftrightarrow O_2^{\bullet-}$: −0.92 V vs. Ag/AgNO3

$O_2^{\bullet-} + CO_2 \rightarrow {}^{\bullet}OOC(=O)O^-$

${}^{\bullet}OOC(=O)O^- + CO_2 \rightarrow {}^{\bullet}OOC(=O)OC(=O)O^-$

${}^{\bullet}OOC(=O)OC(=O)O- + O_2^{\bullet-} \rightarrow {}^-OOC(=O)OC(=O)O^- + O_2$

(in bulk electrolyte close to the electrode)

${}^-OOC(=O)OC(=O)O^- + O_2^{\bullet-} \rightarrow 2CO_3^{2-} + 2O_2$

(in bulk electrolyte close to the electrode)

Similar to the reaction using the Ag electrode, the DRIFTS measurements with the Cu electrode showed a pair of peaks at 1600 and 1670 cm^{-1}, indicating

that asymmetric peroxydicarbonate is generated as an intermediate of the electrochemical reduction of CO_2 and O_2 in the bulk electrolyte (Fig. 3e). The peak ascribed to carbonate was intensified by changing the potential from –1.5 V to 0.0 V, which also suggests that the reaction between asymmetric peroxydicarbonate and $O_2^{\bullet-}$ proceed in the bulk electrolyte. A plausible explanation based on these observations, is that asymmetric peroxydicarbonate and $O_2^{\bullet-}$ remain in the bulk electrolyte relatively close to the Cu electrode, different from the reaction using the Ag electrode.

Finally, the reaction on SUS 316L was considered to be as follows:

(11) CO_2/O_2 reduction on the SUS 316L electrode

$O_2 + e^- \leftrightarrow O_2^{\bullet-}$: −0.92 V vs. $Ag/AgNO_3$

$O_2^{\bullet-} + CO_2 \rightarrow {}^{\bullet}OOC(=O)O^-$

${}^{\bullet}OOC(=O)O^- + O_2^{\bullet-} \rightarrow {}^-OOC(=O)O^- + O_2$

${}^-OOC(=O)O^- + CO_2 \rightarrow {}^-OC(=O)OOC(=O)O^-$

(on the electrode surface)

On the SUS 316L electrode, the product of the electrochemical reduction of CO_2 and O_2 is peroxydicarbonate, as determined by DRIFTS measurements and the evaluation of the electron utilization rate, as described above. Contrary to the results of the DRIFTS measurements with the Ag or Cu electrodes, the doublet observed around 1600~1700 cm^{-1} at negative potential was not detected with the SUS 316L electrode; hence, we concluded that the observed peroxydicarbonate is symmetrical. Importantly, the DRIFTS measurement results, which did not change between –1.5 V and 0.0 V, clearly indicate that a series of reactions proceeds on the surface of the SUS 316L electrode. According to Zhao et al., the electrochemical reduction of CO_2 and O_2 on the electrode surface tends to proceed via a symmetric peroxydicarbonate intermediate, which supports our conclusion[17].

The reactions on the surface of the SUS 316L electrode are worthy of particular attention because these reactions differ from those on the other electrodes. In addition, the CV measurements with this electrode produced interesting results, namely that the onset potential for reduction in the gas mixture containing 50% CO_2 (50% CO_2, 10% O_2 and 40% N_2) was lower on negative side than that in (21% O_2 and 79% N_2) or CO_2 alone. We considered the CO_2 and O_2 adsorption energies on metal electrodes to clarify the characteristic reaction behavior on the SUS 316L electrode. Previous studies[31,34,50] which calculated CO_2 and O_2 adsorption energies evidently showed that most metal substrates other than Fe_2O_3 have neutral adsorption energies for CO_2 whereas the O_2 adsorption energies vary depending on the type of substrate. Among the metal substrates, Ni or Rh substrates have large O_2 adsorption energies. Reportedly, the oxygen adsorption energy is correlated with the activity of the O_2 reduction reaction (ORR), in the form of a volcano-type relationship[33,51]. The CV measurements in the mixed gas (21% O_2 and 79% N_2) atmosphere using a Ni electrode in our study also indicated low activity toward O_2. On the other hand, in the CV measurements using the SUS 316L electrode, a reduction current to O_2 was observed. As mentioned above, as a result of the thin layer of Fe_2O_3 on the surface of the SUS 316L, the O_2 adsorption energy of this electrode is lower than that of Ni[34], the reason for the activity of SUS 316L toward O_2 in our CV measurement. The lower onset potential for reduction on the negative side in the gas mixture containing 50% CO_2 than that in other gases or gas mixtures in the CV measurements, was assumed to be a consequence of the presence of CO_2 in the vicinity of O_2 on the SUS 316L electrode. Because the Fe_2O_3 layer on the surface of SUS 316L has large adsorption energies for both CO_2 and O_2, the correlation differs markedly from that of other substrates. In other words, as SUS 316L allows O_2 and CO_2 to react quasi-simultaneously on the surface, the reduction potential is close to the theoretical value of O_2 reduction. Similarly, the Ag electrode also seems to change the waveform of the CV measurement depending on the presence or absence of CO_2 in the gas mixture; however, this is considered to stem from the electrochemical reduction of CO_2 because the CV waveform in coexisting CO_2 and O_2 is similar to that in CO_2 alone.

In summary, we elucidated the mechanism whereby dilute CO_2 undergoes electrochemical reduction in aprotic solution using our custom-designed electrochemical reaction system ***ACEMS***, which enables changes in the CO_2 concentration and formation of chemical substances to be monitored. The mechanism was validated with three representative electrodes, Ag, Cu, and SUS 316L, and took into consideration that the surface of SUS 316L consisted of Fe_2O_3, as established by XPS and cross-sectional STEM analysis. The results obtained with ***ACEMS*** suggested that the production of CO and carbonate on the Ag or Cu electrodes proceeded via disproportionation, whereas oxalate was generated on the SUS 316L electrode in the electrochemical reaction in an atmosphere of 400 ppm CO_2/N_2 (400 ppm CO_2 and 99.96% N_2). In synthetic air (400 ppm CO_2, 21% O_2, and 79% N_2), the reaction pathways for the Ag or Cu electrodes are more complicated than those in the absence of O_2. This showed that the electrochemical reduction of CO_2 and O_2 proceeds via the asymmetric peroxydicarbonate intermediate to generate CO and/or carbonate. The intermediate is inferred to be produced on the electrodes and diffuse offshore into the ionic liquid, as confirmed by two spectroscopic techniques, DRIFTS and Raman measurements. On the SUS 316L electrode, symmetric peroxycarbonate was verified to be generated as the final product in the electrochemical reduction of CO_2 and O_2, not only by using DRIFTS measurements but also by estimating the rate of electron utilization in ***ACEMS***. With reference to previous studies, the electrochemical reaction pathways are deduced to be dependent on the CO_2 and/or O_2 adsorption energies against substrates. Although we expect that this research alone will contribute to the development of studies of the electrochemical capture/release and conversion of dilute CO_2, we are currently trying to perform SHINERs measurements and DFT calcualations to elucidate in more detail the mechanism of electrochemical reduction of CO_2 and O_2 on any metal substrates. We also believe that our future works can provide more pratical materials, methods and systems for directly reducing CO_2 from air and exhaust gases.

References

[1] a) G.-R. Walther, E. Post, E. Post, A. Menzel, C. Parmesan, T. J. C. Beebee, J.-M. Fromentin, O. Hoegh-Guldberg, F. Bairlein, Nature 2002, 416, 389–395; b) M. Mikkelsen, M. Jorgensen, F. C. Krebs, Energy Environ. Sci. 2010, 3, 43–81; c) M. E. Boot-Handford, J. C. Abanades, E. J. Anthony, M. J. Blunt, S. Brandani, N. M. Dowell, J. R. Fernández, M.-C. Ferrari, R. Gross, J. P. Hallett, R. S. Haszeldine, P. Heptonstall, A. Lyngfelt, Z. Makuch, E. Mangano, R. T. J. Porter, M. Pourkashanian, G. T. Rochelle, N. Shah, J. G. Yaoa, P. S. Fennell, Energy Environ. Sci. 2014, 7, 130–189.

[2] a) J. Newman, P. G. Hoertz, C. A. Bonino, J. A. Trainham, J. Electrochem. Soc. 2012, 159, A1722–1729; b) J. Qiao, Y. Liu, F. Hong, J. Zhang, Chem. Soc. Rev. 2014, 43, 631–675; c) R. Schlögl, ChemSusChem 2010, 3, 209–222; d) Y.Hori, K. Kikuchi, S. Suzuki, Chem. Lett. 1985, 14, 1695–1698; e) Z. Sun, H. Yin, K. Liu, S. Cheng, G. K. Li, S. Kawi, H. Zhao, G. Jia, Z. Yin, SmartMat 2022, 3, 68–83; f) J. Qiu, H. Zhao, Y. Lei, SmartMat 2022, 3, 447–473.

[3] a) W. D. Jones, J. Am. Chem. Soc. 2020, 142, 4955–4957; b) E. S. Sanz-Pérez, C. R. Murdock, S. A. Didas, C. W. Jones, Chem. Rev. 2016 116, 11840–11876; c) K. S. Lackner, S. Brennan, J. M. Matter, A.-H. A. Park, A. Wright, B. van der Zwaan, Proc. Natl. Acad. Sci. U. S. A. 2012, 109, 13156–13162.

[4] a) S. Voskian, T. A. Hatton, Energy Environ. Sci. 2019, 12, 3530–3547; b) Y. Liu, H.-Z. Ye, K. M. Diederichsen, T. V. Voorhis, T. A. Hatton, Nat. Commun. 2020, 11, 2278; c) F. Simeon, M. C. Stern, K. M. Diederichsen, Y. Liu,

H. J. Herzog, T. A. Hatton, J. Phys. Chem. C 2022, 126, 1389–1399.

[5] a) Y. Yamazaki, M. Miyaji, O. Ishitani, J. Am. Chem. Soc. 2022, 15, 6640–6660; b) S. V. Daele, L. Hintjens, J. Van den Hoek, S. Neukermans, N. Daems, J. Hereijgers, T. Breugelmans, J. CO_2 Util. 2022, 65, 102210; c) S. V. Daele, L. Hintjens, J. Van den Hoek, S. Neukermans, N. Daems, J. Hereijgers, T. Breugelmans, J. CO_2 Util. 2022, 65, 102210.

[6] Y. Qiao, J. Yi, S. Wu, Y. Liu, S. Yang, P. He, H. Zhou, Joule 2017, 1, 359–370.

[7] L. Sun, G. K. Ramesha, P. V. Kamat, J. F. Brennecke, Langmuir 2014, 30, 6302–6308.

[8] J. Xie, Q. Liu, Y. Huang, M. Wu, Y. Wang, J. Mater. Chem. A 2018, 6, 13952–13958.

[9] a) S. Ikeda, T. Takagi, K. Ito, Bull. Chem. Soc. Jpn. 1987, 60, 2517–2522; b) A. Bagger, O. Christensen, V. Ivaništšev, J. Rossmeisl, ACS Catal. 2022, 12, 2561–2568; c) O. Kuntyi, G. Zozulya, M. Shepida, J. Chem. 2022, 1306688.

[10] H. Yamamoto, T. Mashino, T. Nagano, M. Hirobe, Tetrahedron Lett. 1989, 30, 4133–4136.

[11] S. Jin, M. Wu, Y. Jing, R. G. Gordon, M. J. Aziz, Nat. Commun. 2022, 13, 2140.

[12] A. Halilu, M. Hayyan, M. K. Aroua, R. Yusoff, H. F. Hizaddin, Phys. Chem. Chem. Phys. 2021, 23, 1114–1126.

[13] a) A. Halilu, M. Hayyan, M. K. Aroua, R. Yusoff, H. F. Hizaddin, W. J. Basirun, J. Environ. Chem. Eng. 2021, 9, 105285; b) A. Halilu, M. Hayyan, M. K. Aroua, R. Yusoff, H. F. Hizaddin, ACS Appl. Mater. Interfaces 2019, 11, 25928–25939; c) C. Xiao, X. Zeng, J. Electrochem. Soc. 2013, 160, H749–H756.

[14] S. Mondal, R. B. Jethwa, B. Pant, R. Hauschild, S. A. Freunberger, Faraday Discuss. 2024, 248, 175–189.

[15] a) J. L. Roberts Jr., T. S. Calderwood, D. T. Sawyer, J. Am. Chem. Soc. 1984, 106, 4667–4670; b) P. A. Giguère, D. Lemaire, Can. J. Chem. 1972, 50, 1472–1477.

[16] Y. Qiao, J. Yi, S. Guo, Y. Sun, S. Wu, X. Liu, S. Yang, P. Hec, H. Zhou, Energy Environ. Sci. 2018, 11, 1211–1217.

[17] Z. Zhao, Y. Su, Z. Peng, J. Phys. Chem. Lett. 2019, 10, 322–328.

[18] K. Takechi, T. Shiga, T. Asaoka, Chem. Commun. 2011, 47, 3463–3465.

[19] S. K. Das, S. Xu, L. A. Archer, Electrochem. Commun. 2013, 27, 59–62.

[20] W. I. Al Sadat, L. A. Archer, Sci. Adv. 2016, 2, e1600968.

[21] a) Y. Wang, L. Hao, M. Bai, J. Electrochem. Soc. 2021, 168, 020524; b) F. M. Mota, J.-H. Kang, Y. Jung, J. Park, M. Na, D. H. Kim, H. R. Byon, Adv. Energy Mater. 2020, 10, 1903486; c) Z. Xie, X. Zhang, Z. Zhang, Z. Zhou, Adv. Mater. 2017, 29, 1605891; d) K. Chen, G. Huang, J.-L. Ma, J. Wang, D.-Y. Yang, X.-Y. Yang, Y. Yu, X.-B. Zhang, Angew. Chem. 2020, 132, 16804–16810; e) L. Zou, Y. Jiang, J. Cheng, Z. Wang, L. Jia, B. Chi, J. Pu, L. Jian, ChemCatChem 2019, 11, 3117–3124; f) W. Yin, A. Grimaud, F. Lepoivre, C. Yang, J. M. Tarascon, J. Phys. Chem. Lett. 2017, 8, 214–222; g) Y.Yoo, G. Lee, M.-G. Jeong, H.-G. Jung, S. Shin, D. Byun, T. Yim, H.-D. Lim, J. Energy Chem. 2022, 65, 646–653; h) T. Wang, X. Pan, J. Chen, Y. Chen, J. Phys. Chem. Lett. 2021, 12, 4799–4804; i) N. Kunanusont, Y. Shimoyama, ACS Appl. Energy Mater. 2020, 3, 4421–4431; j) K. Iputera, J.-Y. Huang, S.-C. Haw, J.-M. Chen, S.-F. Hu, R.-S. Liu, J. Mater. Chem. A 2022, 10, 3460–3468; k) F. M. Mota, Y. Kim, H. Hong, S. Yu, S. Lee, D. H. Kim, ACS Appl. Energy Mater. 2022, 5, 2150–2160; l) H.-K. Lim, H.-D. Lim, K.-Y. Park, D.-H. Seo,H. Gwon,J. Hong, W. A. Goddard III, H. Kim, K. Kang, J. Am. Chem. Soc. 2013, 135, 9733–9742; m) J.-H. Kang, J. Park, M. Na, R. H. Choi, H. R. Byon, ACS Energy Lett. 2022, 7, 4248–4257; n) S. Zhang, M. J. Nava, G. K. Chow, N. Lopez, G. Wu, D. R. Britt, D. G. Nocera, C. C. Cummins, Chem. Sci. 2017, 8, 6117–6122.

[22] a) G. Iijima, T. Inomata, H. Yamaguchi, M. Ito, H. Masuda, ACS Catal. 2019, 9, 6305–6319; b) G. Iijima, J. Naruse, H. Shingai, K. Usami, T. Kajino, H. Yoto, Y. Morimoto, R. Nakajima, T. Inomata, H. Masuda, Energy Fuels 2023, 37, 2164–2177.

[23] a) Z. Wang, L. Zhang, X. Tang, Z. Zhang, M. Lu, Appl. Surf. Sci. 2017, 423, 457–464; b) J. Poloprudský, A. Chlupová, I. Šulák, T. Kruml, S. Hloch, Materials 2021, 14, 5212; c) T. Tanabe, S. Imoto, Trans. Jpn. Inst. Metal 1979, 20, 507–515.

[24] a) B. A. Rosen, A. Salehi-Khojin, M. R. Thorson, W. Zhu, D. T. Whipple, P. J. A. Kenis, R. I. Masel, Science 2011, 334, 643–644; b) B. Gorodetsky, T. Ramnial, N. R. Branda, J. A. C. Clyburne, Chem. Commun. 2004, 1972–1973; c) A. Fortunati, F. Risplendi, M. R. Fiorentin, G. Cicero, E. Parisi, M. Castellino, E. Simone, B. Iliev, T. J. S. Schubert, N. Russo, S. Hernández, Commun. Chem. 2023, 6, 84.

[25] F.M. Vitucci, F. Trequattrini, O. Palumbo, J.-B. Brubach, P. Roy, A. Paolone, Vib. Spectrosc. 2014, 74, 81–87.

[26] a) M. Hayyan, M. H. Ibrahim, A. Hayyan, M. Ali Hashim, Braz. J. Chem. Eng. 2017, 34, 227–239; b) M. Hayyan, F. S. Mjalli, M. Ali Hashim, I. M. AlNashef, S. M. Al-Zahrani, K. L. Chooi, J. Electroanal. Chem. 2012, 664, 26–32; c) C. J. Allen, J. Hwang, R. Kautz, S. Mukerjee, E. J. Plichta, M. A. Hendrickson, K. M. Abraham, J. Phys. Chem. C 2012, 116, 20755-20764.

[27] T. A. Galloway, L. J. Hardwick, J. Phys. Chem. Lett. 2016, 7, 2119–2124.

[28] P. M. Radjenovic, L. J. Hardwick, Faraday Discuss. 2018, 206, 379–392.

[29] F. Cai, Z. Hu, S.-L. Chou, Adv. Sustain. Syst. 2018, 2, 1800060.

[30] H. Xing, P. Hu, S. Li, Y. Zuo, J. Han, X. Hua, K. Wang, F. Yang, P. Feng, T. Chang, J. Mar. Sci. Technol. 2021, 62, 80–194.

[31] M. M. Montemore, M. A. van Spronsen, R. J. Madix, C. M. Friend, Chem. Rev. 2018, 118, 2816–2862.

[32] A. Kulkarni, S. Siahrostami, A. Patel, J. K. Nørskov, Chem. Rev. 2018, 118, 2302–2312.

[33] N. V. Long, Y. Yang, C. M. Thi, N. V. Minh, Y. Cao, M. Nogami, Nano Energy 2013, 2, 636–676.

[34] C. Chen, C. Zhao, X. Zhou, J. Chen, L. Chen, F. Li, Vacuum 2021, 188, 110164.

[35] Q. Peng, Y. Qiao, K. Kannari, A. Ge, K. Inoue, S. Ye, J. Phys. Chem. C 2020, 124, 15781–15792.

[36] a) P.-F. Zhang, J.-Y. Zhang, T. Sheng, Y.-Q. Lu, Z.-W. Yin, Y.-Y. Li, X.-X. Peng, Y. Zhou, J.-T. Li, Y.-J. Wu, J.-X. Lin, B.-B. Xu, X.-M. Qu, L. Huang, S.-G. Sun, ACS Catal. 2020, 10, 1640–1651; b) Y. Xing, Y. Yang, D. Li, M. Luo, N. Chen, Y. Ye, J. Qian, L, Li, D. Yang, F. Wu, R. Chen, S. Guo, Adv. Mater. 2018, 30, 1803124.

[37] S. Subramanian, K.R. Athira, M. A. Kulandainathan, S. S. Kumar, R.C. Barik, J. CO2 Util. 2020, 36, 105–115.

[38] M. Wu, J. Y. Kim, H. Park, D. Y. Kim, K. M. Cho, E. Lim, O. B. Chae, S. Choi, Y. Kang, J. Kim, H.-T. Jung, ACS Appl. Mater. Interfaces 2020, 12, 32633–32641.

[39] a) C. Yang, K. Guo, D. Yuan, J. Cheng, B. Wang, J. Am. Chem. Soc. 2020, 142, 6983–6990; b) Y. Hou, J. Wang, L. Liu, Y. Liu, S. Chou, D. Shi, H. Liu, Y. Wu, W. Zhang, J. Chen, Adv. Funct. Mater. 2017, 27, 1700564; c) A. Gennaro, A. A. Isse, M.-G. Severin, E. Vianello, I. Bhugun, J.-M. Savéant, J. Chem. Soc., Faraday Trans. 1996, 92, 3963–3968.

[40] a) M. C. Figueiredo, I. Ledezma-Yanez, M. T. M. Koper, ACS Catal. 2016, 6, 2382–2392; b) T. Mairegger, H. Li, C. Grießer, D. Winkler, J. Filser, N. G. Hörmann, K. Reuter, J. Kunze-Liebhäuser, ACS Catal. 2023, 13, 5780–5786.

[41] F.Li, L. Koopal, W. Tan, Sci. Rep. 2018, 8, 2060.

[42] M. E. G. Winkler, R. H. Gonçalves, A. F. Rubira, ACS Omega 2022, 7, 45067–45076.

[43] M. He, C. Li, H. Zhang, X. Chang, J. G. Chen, W. A. Goddard III, M.-j. Cheng, B. Xu, Q. Lu, Nat. Commun. 2020, 11, 3844.

[44] M. Moradzaman, G. Mul, ACS Catal. 2020, 10, 8049–8057.

[45] A. Paredes-Nunez, I. Jbir, D. Bianchi, F. C. Meunier, Appl. Catal. A 2015, 495, 17–22.

[46] a) Y. Ichinohe, T. Wadayama, A. Hatta, J. Raman Spectrosc. 1995, 26, 335–340; b) L. W. H. Leung, M. J. Weaver, Langmuir 1988, 4, 1076–1083.

[47] W. Lian, L. Wang, Y. Song, H. Yuan, S. Zhao, P. Li, L. Chen, Electrochim. Acta 2009, 54, 4334–4339.

[48] A. Boltasseva, H. A. Atwater, Science 2011, 331, 290–291.

[49] a) A. Haryanto, C. W. Lee, Nano Convergence 2022, 9, 9; b) G. Frens, Nat. Phys. Sci. 1973, 241, 20–22.

[50] a) X. Liu, L. Sun, W. Deng, J. Phys. Chem. C 2018, 122, 8306–8314; b) P. Błoński, A. Kiejna, J. Hafner, Surf. Sci. 2005, 590, 88–100; c) H. Wang, X. Nie, Y. Chen, X. Guo, C. Song, J. CO_2 Util. 2018, 26, 160–170; d) L. Zhou, A. Kandratsenka, C. T. Campbell, A. M. Wodtke, H. Guo, Angew. Chem., Int. Ed. 2019, 58, 6916–6920; e) S. Matsuda, T. Mukai, S. Sakurada, N. Uchida, M. Umeda, New J. Chem. 2019, 43, 13717–13720; f) C. Breyer, D. Reichert, J. Seidel, R. Hüttl, F. Mertensb, S. Kureti, Phys. Chem. Chem. Phys. 2015, 17, 27011–27018; g) M. Mohammadi, E. Pakizeh, Mater. Sci. Eng. B 2023, 297, 116752; h) P. Błoński, A. Kiejna, J. Hafner, Phys. Rev. B 2008, 77, 155424.

[51] a) Y.-C. Lu, H. A. Gasteiger, Y. Shao-Horn, J. Am. Chem. Soc. 2011, 133, 19048–19051; b) P. Lang, N. Yuan, Q. Jiang, Y. Zhang, J. Tang, Energy Technol. 2020, 8, 1900984.

著者

飯島 剛
いいじま ごう

マテリアル研究部　博士（工学）
電気化学材料の開発に従事

杉浦 恭輔
すぎうら きょうすけ

先端技能開発部
材料開発における環境開発に従事

森下 賢一
もりした けんいち

先端技能開発部
材料開発における環境開発に従事

眞貝 孟
しんがい はじめ

マテリアル研究部　博士（工学）
材料開発基盤の技術開発に従事

成瀬 淳一
なるせ じゅんいち

マテリアル研究部
電気化学材料の開発に従事

世登 裕明
よとう ひろあき

マテリアル研究部　博士（工学）
無機機能材料の開発に従事